Applied Clay Science 249 (2024) 107236

Contents lists available at ScienceDirect

Applied Clay Science

journal homepage: www.elsevier.com/locate/clay

Research Paper

# Diving into micro- and macroscopic properties of egg-tempera paint based on Sienna pigment

Floriane Gerony [a,b], Laurence de Viguerie [a], Côme Thillaye du Boullay [a], Fabrice Gaslain [c], Bruno Lanson [d], Camille Colin [a], Laurent Michot [b], Anne-Laure Rollet [b], Guillaume Mériguet [b], Maguy Jaber [a,e,*]

[a] Sorbonne Université, CNRS UMR 8220, LAMS, case courrier 225, 4 pl. Jussieu 75252 Paris cedex 05, France
[b] Sorbonne Université, CNRS UMR 8234, PHENIX, case courrier 51, 4 pl. Jussieu 75252 Paris cedex 05, France
[c] Mines Paris, Université PSL, Centre des Matériaux (MAT), UMR 7633 CNRS, 91003 Evry, France
[d] Univ. Grenoble Alpes, CNRS, Univ. Savoie Mont Blanc, IRD, Univ. Gustave Eiffel, ISTerre, F-38000 Grenoble, France
[e] Institut Universitaire de France, Paris, France

ARTICLE INFO

*Keywords:*
Tempera paint
Sienna earth
Yolk
Lecithin
Relaxometry
Rheology

ABSTRACT

Egg-tempera painting was a pictorial technique widespread in the Middle Ages. In this work, Sienna earth and yolk have been used to formulate tempera paints according to historical recipes. Micro- and macroscopic properties were investigated to understand the interactions between the pigment and the binder. The pigment, inorganic part of the paint, was characterized by X-Ray Diffraction (XRD), thermal analysis (TG-DTA), Fourier Transform Infrared (FT-IR) Spectroscopy, granulometry, as well as Scanning Electron Microscopy (SEM). Then lecithin adsorption onto pigment particles was probed to understand yolk interaction with Sienna earth, pure kaolinite and goethite particles. NMR-Relaxometry was used to investigate the behavior and accessibility of the mineral surfaces to yolk and water. Macroscopic rheological properties of the paint systems were finally investigated.

## 1. Introduction

Until the end of the 15th century, the predominant painting technique was *tempera*, i.e. a mixture of a colored pigment with an aqueous binder. In Western Europe, between the 13th and 15th centuries, the most commonly used aqueous binder was egg yolk and many artists therefore painted with an egg-tempera technique. Some tempera binder recipes are reported in medieval manuscripts. For instance, in the famous manuscript "Libro Del Arte", the apprentice painter Cennino Cennini (1390–1437) described the mixing of egg yolk and pigments, and mentioned that such a mixture could be used to paint a wide range of materials: walls, panels, or iron among others (Cennini and Broecke, 2015). Numerous pigments both synthetic and natural were employed by artists at that time. Among them, as mentioned in several medieval manuscripts (Mayer and Sheehan, 1991; Merrifield, 1999; Clarke, 2011; Cennini and Broecke, 2015), natural earths and ochres were particularly popular, as they were used to form the base of the first paint layers of flesh tones. Sienna earth is a typical example of this family of pigments. Most of these pigments are complex mineral mixtures. Sienna earth mainly contains goethite, various clay minerals (kaolinite, smectite, illite….), and additional accessory minerals, the nature of which depends on the geological setting (Helwig, 1998; Grygar et al., 2003; Hradil et al., 2003).

Identification techniques classically used on tempera artworks and mock-ups do not provide any information about the interactions between pigments and binders, even though these interactions are of prime importance since they govern the final properties of the paints. Still, some spectroscopic analyses have been carried out in mock-ups after drying (Meilunas et al., 1990; Mazzeo et al., 2008; Navas et al., 2010; Romero-Pastor et al., 2011; Manea et al., 2012). In the case of egg-tempera paint with Sienna, some interactions between the pigments and egg yolk could be evidenced from the spectral evolution of the aliphatic and aromatic C—H regions of aromatic amino acids (Romero-Pastor et al., 2011). Fanost and coworkers studied green earth tempera paints (Fanost, 2019; Fanost et al., 2022) and showed that the combination of NMR-relaxometry and rheology measurements on fresh paints

* Corresponding author at: Sorbonne Université, CNRS UMR 8220, LAMS, case courrier 225, 4 pl. Jussieu 75252 Paris cedex 05, France.
*E-mail address:* maguy.jaber@sorbonne-universite.fr (M. Jaber).

https://doi.org/10.1016/j.clay.2023.107236
Received 14 July 2023; Received in revised form 29 November 2023; Accepted 15 December 2023
Available online 20 January 2024

provides fruitful information on the binder-pigment network that controls to a large extent the rheological properties of paints and consequently the way they flow and spread on canvases (Salvant Plisson et al., 2014) which often explains why painters chose specific formulations.

The present paper deals with egg-tempera painting with Sienna earth as pigment. After characterizing in details the structural and morphological properties of Sienna by various techniques (XRD, FTIR, Laser diffraction, Gas adsorption, Thermo Gravimetric Analysis, Scanning Electron Microscopy), we focused on the interactions between the pigment and the binder, analyzing the adsorption of lecithin, one of the main components of egg yolk, on the pigments and probing interfaces between binder and pigment with NMR relaxometry. Sienna earth being a complex natural system, we also investigated the possibility to use a mixture of pure minerals as a synthetic Sienna. The rheological properties of natural Sienna tempera paint were then compared to the ones of tempera paints based on the reconstituted Sienna as well as its individual components. Model systems are often employed in physico-chemical studies but, to the best of our knowledge, it is the first use of a model pigment in the cultural heritage field.

## 2. Materials and methods

### 2.1. Materials

Italian raw Sienna (#40400) and synthetic goethite (#48000, purity >99.4%) were supplied by Kremer Pigmente (Germany). Clay minerals kaolinite (KGa-1b, purity kaolin 95–100%, quartz 1–2%) and montmorillonite (Texas STx-1, purity montmorillonite 95–100%, quartz 1–5%) were purchased from The Clay Minerals Society (USA). Calcite (purity >99%) was obtained from Sigma-Aldrich.

Reconstituted Sienna is the mix of the pure minerals with proportions by weight of 37% kaolinite, 27% goethite, 14% montmorillonite and 22% calcite.

Fresh organic hen eggs were purchased from a local store.

Soybean L-α-Lecithin (CAS 8002-43-5 – Calbiochem®) was obtained from Sigma-Aldrich and was solubilized in ethanol denatured ≥96% (CAS 64–17-5, GPR RECTAPUR®) from VWR BDH Chemicals. The headgroup area of lecithin ($a0 = 0.58\ nm^2$) was determined with Avogadro software (Version 1.2.0) using Universal Force Field (UFF) and is consistent with literature values (Brouillette et al., 1982; Israelachvili, 2011).

### 2.2. Sample preparation

#### 2.2.1. Adsorption isotherms

As lecithin is not soluble in water, it was solubilized into ethanol. 20 mL of lecithin/ethanol solutions (at concentrations in the range 2–100 mM for Sienna and kaolinite and 2–350 mM for goethite) were added to 300 mg of powder in closed flasks and stirred for 24 h. Dispersions were then centrifuged at 4000*g* during 15 min. Solid substrates were analyzed by thermogravimetric analysis coupled with differential thermal analysis (TG-DTA) to determine the charge *Q* (mass of lecithin adsorbed per gram of powder). For Sienna and goethite isotherms, lecithin charge was not directly measurable by TGA analysis because lecithin decomposition and goethite to hematite transition occur in the same temperature range (Fig. 2 and Fig. S2). We estimated the loss of weight due to iron oxides transformation and the remaining loss of weight was assigned to lecithin decomposition.

#### 2.2.2. Paint reconstruction protocol

Paints were formulated after selecting recipes from medieval manuscripts and more recent manuals (Laurie, 1926; Thompson and York, 1962; De L'escalopier, 1977; Mayer and Sheehan, 1991; Merrifield, 1999; Clarke, 2011; Cennini and Broecke, 2015) and further discussion with restorers. A simplified preparation protocol was elaborated to be applicable and reproducible in the laboratory. Pure yolk was obtained by rolling the yolk from one hand to another to remove the white, and by piercing the yolk to eliminate the membrane (Mayer and Sheehan, 1991). In order to improve reproducibility, 3 fresh organic hen egg yolks from the same box were mixed. Tempera binder was prepared by mixing egg yolk (75 wt%) with ultra-pure water (25 wt%).

For rheology measurements, tempera paints were prepared as follows: 3 g of pigment were manually ground into 2 g of ultra-pure water during 2 min with a glass muller. Then 4 g of tempera binder were added to the pigment paste and mixed again with the glass muller during 4 min. In the end, paint systems correspond to $^1/_3$ pigment, $^1/_3$ water and $^1/_3$ egg yolk.

For relaxometry measurements, $^1/_3$ of pigment was dispersed in water or in tempera binder and ground with a glass muller.

### 2.3. Analytical techniques

#### 2.3.1. X-ray diffraction (XRD) and Rietveld refinement

XRD patterns were collected on natural Sienna using a Bruker D8 diffractometer equipped with Co radiation ($\lambda = 1.78897$ Å) operated at 40 kV and 40 mA. Intensities were measured with a Vortex 60EX silicon drift detector (Hitachi High-Tech America) for 8 s per 0.026° 2θ step over the 5–90° 2θ Co Kα angular range. Divergence slit, the two Soller slits, the antiscatter, and resolution slits were fixed at 0.3°, 2.3°, 0.3°, and 0.2°, respectively. Quantitative phase analysis was performed from the Rietveld refinement of XRD data using the Profex software (Doebelin and Kleeberg, 2015). Quantification of the sample amorphous content was also performed from the Rietveld refinement of XRD data after addition of an internal standard (~20 wt% of corundum – α-$Al_2O_3$) to the sample and careful mixing and homogenization.

#### 2.3.2. Scanning electron microscopy (SEM)

Analyses were carried out with a FEI Nova NanoSEM 450 microscope equipped with a FEG source and an immersion lens. Secondary electron imaging was performed with a through-the-lens detector (TLD) between 2 and 5 kV.

#### 2.3.3. Laser diffraction particle size analyzer

Size measurements were performed with a Mastersizer 3000 laser diffraction particle size analyzer with Hydro EV accessory (Malvern Panalytical). Powders were dispersed in water. 3 measurements were made per sample and the values are reported as volume and number distributions.

#### 2.3.4. Gas adsorption

$N_2$ adsorption-desorption isotherms of natural Sienna and goethite were carried out at 77 K on a Micromeritics ASAP 2010 gas analyzer. Prior to the analysis, the samples were outgassed under vacuum at 200 °C for 6 h. Specific surface areas were determined using the BET model.

#### 2.3.5. Thermogravimetric analysis (TGA)

Thermal analyses were performed with a SDT-Q600 (TA Instruments). Approximatively 20 mg of powder were placed in an alumina crucible and a temperature ramp of 5 °C/min was applied from 25 to 1000 °C. Measurements were conducted with an air flow of 75 mL/min.

#### 2.3.6. NMR-relaxometry

Measurements of the water $^1H$ longitudinal relaxation rates $R_1 = 1/T_1$ were performed using a SpinMaster Field Cycling relaxometer (Stelar) in the 0.01–30 MHz frequency range. From 10 kHz to 10 MHz a pre-polarized sequence was used whereas a non-polarized sequence was employed between 10 MHz and 30 MHz (Anoardo et al., 2001). The magnetization curves, built with 16-time increments, exhibit a mono-exponential dependency. Samples were conditioned in glass tubes (10 mm external diameter, 38 mm length) closed by a silicon cap (Fanost

et al., 2020). 30 wt% suspensions of mineral were prepared by grinding the powder in a water with a glass muller. For calcite suspension, which is not very stable, measurements were taken point by point and samples were shaken between each measurement. The sample almost completely filled the tube to prevent evaporation during the experiments. Samples were thermostated at 298 K using regulated air flux.

#### 2.3.7. FT-IR spectroscopy

Fourier-transform infrared (FT-IR) spectra were acquired on a Bruker Tensor 27 spectrometer. Transmission measurements were performed using KBr (CAS 7758-02-3 – Uvasol®, for IR spectroscopy, Merck, Germany) transparent pellets that were obtained by applying a weight of 10 tons on mixtures of about 2 mg of powder and 100 mg of anhydrous KBr previously crushed and homogenized in an agate mortar. A 32-scan average spectrum was recorded from 4000 to 400 $cm^{-1}$ with a resolution of 4 $cm^{-1}$. Baseline subtraction and peak indexation were performed using OriginPro 9.0 software.

#### 2.3.8. Rheology

Rheological measurements were carried out using a Thermo Scientific HAAKE MARS 40 rheometer. A sandblasted titanium 35 mm-diameter and 2°-angle cone/plate geometry was used. Tests were performed at 25 °C using a plastic hood to avoid drying of the paint during the measurements. All tests were carried out at least twice on the same paint and on the same day. Error bars were computed as the standard deviation of these measurements.

Flow measurements were performed by increasing and decreasing the shear rate between $\dot{\gamma} = 0.01$ and 1000 $s^{-1}$. Because back and forth measurements were almost superimposed (i.e. thixotropic effects are negligible), only the downward ramp is plotted in the following; exception for kaolinite where the upward ramp is shown because the low viscosity of the suspension caused sedimentation during the measurement.

Strain sweep measurements were performed at increasing stresses from $\tau = 0.01$ to 100 Pa at a constant oscillatory frequency of 1 Hz.

Frequency sweep measurements were carried out at constant stress $\tau$ =0.1 Pa (value chosen in the linear viscoelastic regime) with decreasing frequency from 100 to 0.1 Hz.

## 3. Results and discussion

### 3.1. Natural Sienna characterization and reconstruction

The X-ray diffraction pattern of natural Sienna (Fig. 1) reveals the presence of numerous mineral phases, the relative proportions of which were deduced from a Rietveld refinement of XRD data (Table 1).

Natural Sienna is mainly composed of clay minerals (~33% kaolinite and ~12% smectite) and iron oxide (~24% goethite). A significant amount of calcite (~13%) is also present in the pigment. The systematic presence of broad and sharp lines corresponding to goethite (Fig. S1) indicated the coexistence of two goethite populations in natural Sienna. Positions of sharp lines are typical of ideal goethite whereas broad lines are systematically shifted towards higher angle (Fig. S1) most likely owing to common Al-for-Fe substitutions in goethite (Schulze, 1984; Schwertmann and Cornell, 2000). The associated decrease of volume unit cell (from 0.1387 $nm^3$ in ideal goethite to 0.1366 $nm^3$ in Al-substituted goethite) indicates the presence of 10–15 mol% Al in the prevailing (~75% of the total goethite content in natural Sienna) Al-substituted goethite (Schwertmann and Carlson, 1994). Peak

**Table 1**
Quantitative phase analysis of natural Sienna determined by Rietveld refinement.

| Minerals | %wt |
|---|---|
| Kaolinite | 32.7(5) |
| Goethite | 23.5(4) |
| Calcite | 12.9(2) |
| Smectite | 12.1(5) |
| Anatase | 2.7(1) |
| Quartz | 1.6(1) |
| Gypsum | 0.7(1) |
| Amorphous | 13.8(11) |

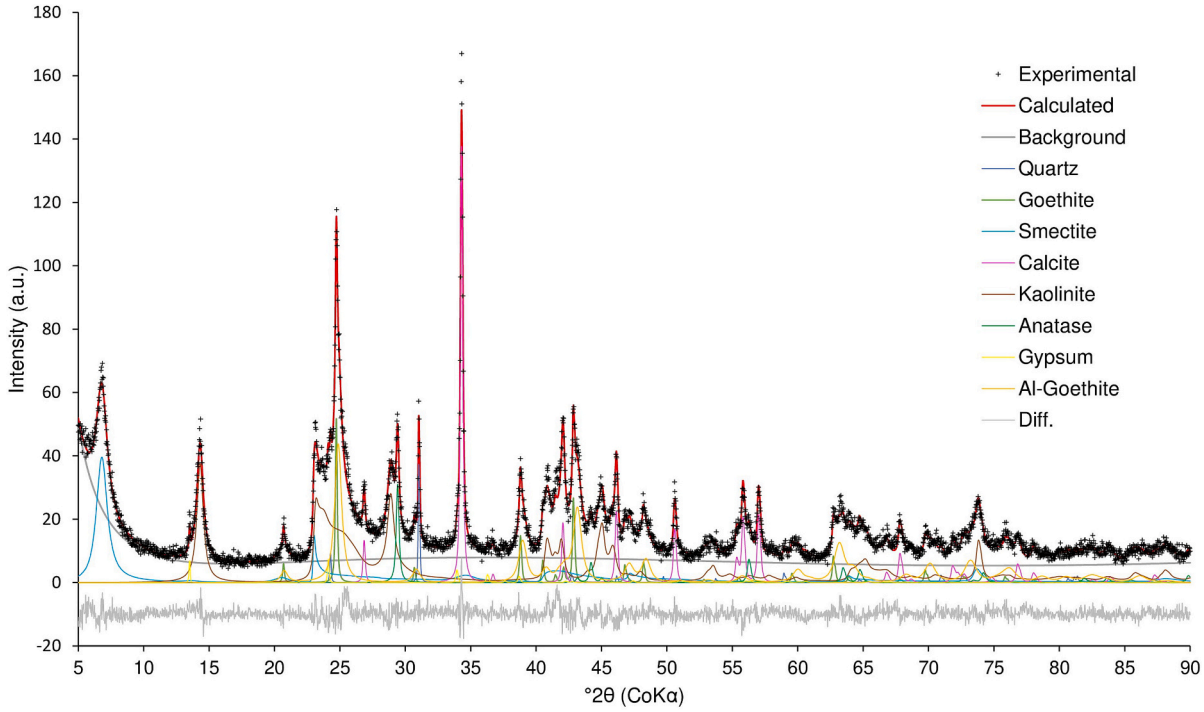


**Fig. 1.** Rietveld refinement results (experimental pattern in black, calculated pattern in red, difference in grey) of natural Sienna. Rp = 7.77%, Rwp = 10.12%, Rexp = 8.41%, GoF = 1.20. (For interpretation of the references to colour in this figure legend, the reader is referred to the web version of this article.)

broadening associated to Al-for-Fe substitution in goethite indicates a decrease of the average coherent scattering domain size from ~80 nm to ~15 nm.

The IR spectrum of natural Sienna is presented in Fig. 2a. Vibration bands corresponding to kaolinite, goethite and calcite can be identified in this spectrum. The presence of kaolinite is evidenced by the Si—O stretching band at 1034 $cm^{-1}$ and the Si-O-Al band at 1011 $cm^{-1}$. The two OH stretching bands at 3695 and 3620 $cm^{-1}$ that correspond to structural hydroxyls can also be linked to the presence of kaolinite. Bands corresponding to goethite are also observed particularly in the low wavenumber region where signals at 538, 469 and 430 $cm^{-1}$ correspond to Fe—O, in addition of those at 3423 and 3238 $cm^{-1}$ assigned to the hydroxyl groups. However, the latter bands could also be related to the presence of smectite. Finally, the presence of calcite in the sample is evidenced by the occurrence of the carbonate stretching vibration band at 1425 $cm^{-1}$ (Helwig, 1998; Bikiaris et al., 2000; Genestar and Pons, 2005; Manasse and Mellini, 2006).

The TG-DTA curve of natural Sienna (Fig. 2b) displays various weight losses. The features below 150 °C can be assigned to the outgassing of physisorbed water. The event around 285 °C corresponds to the goethite/hematite transition (Manasse and Mellini, 2006). In quantitative terms, this event corresponds to a weight loss of 2.5% of the initial mass. The weight loss for pure goethite would correspond to 10%, leading to an estimation of 25% of goethite in natural Sienna, a value extremely close to the one deduced from the Rietveld refinement. The weight losses around 465 °C and 675 °C can be assigned to respectively kaolinite dehydroxylation and calcite decomposition (Genestar Juliá and Pons Bonafé, 2004). There again the quantitative results are consistent with mineral proportions deduced from the Rietveld analysis.

The particle size distribution of Sienna was determined by laser diffraction (Fig. 3). The volume distribution (dashed line) exhibits a wide range of sizes and is centered around 25 µm. However, such a representation of the results tends to favor the larger particles and it is relevant to plot the number distribution (solid line). This shows that most particles in Sienna are submicronic in size with a distribution centered around 1 µm. It must be recalled however that laser diffraction results assume the presence of spherical objects, which is obviously not the case here as shown by SEM images (Fig. 4). The sizes determined should then be considered as indicative rather than a precise value.

Scanning Electron Microscopy (SEM) micrographs of natural Sienna (Fig. 4) reveal two main crystal morphologies. Indeed, platy particles and needle-like ones can be observed. EDX analyses (not shown) reveal that the platy particles contain mainly silicon, aluminum and/or calcium whereas the needle-like ones are iron-rich. It then appears that the platelets can be assigned to clay minerals and the needles to goethite. In

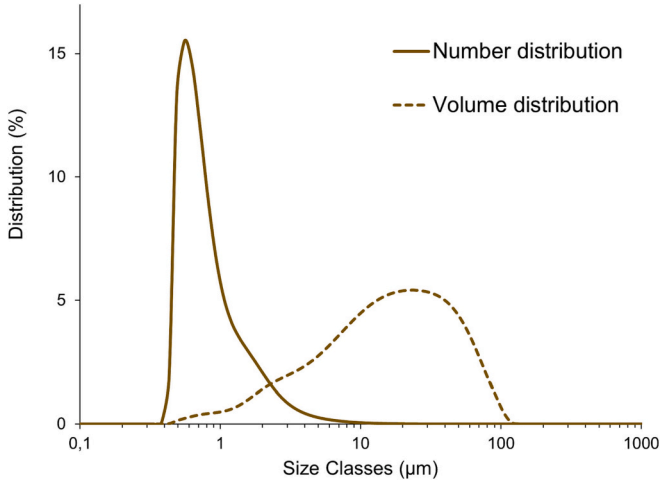


**Fig. 3.** Size distribution in volume and in number of Sienna particles in water.

terms of size, the goethite particles are about 1 µm long and 0.1 µm wide whereas the platelets have a diameter (d) of about 100 nm and a thickness (e) of about 20 nm, i.e. an aspect ratio d/e of 0.2. Literature reports that natural Sienna can contain low amounts of manganese oxide, giving it a brownish hue (Hradil et al., 2003), and that arsenic is sometimes present in Sienna samples (Manasse and Mellini, 2006). These two elements were not observed in the Sienna used in the present study.

The specific surface area (SSA) of natural Sienna determined by gas adsorption is 45.8 $m^2.g^{-1}$, a large value that appears consistent with the submicron size of most particles deduced from SEM images and laser diffraction results.

Sizes and morphological properties of pure goethite and pure kaolinite later used as model systems in this study have also been characterized. Size measurements of both minerals are compared to those obtained for natural Sienna in Fig. 5. The range of sizes of both goethite and kaolinite is similar to that of natural Sienna, most particles being submicronic (Fig. 5 right).

SEM images of pure minerals goethite and kaolinite are presented on Fig. 6. The shape and size of goethite particles are similar to those of the needle-like grains observed in natural Sienna (about 1 µm × 0.1 µm), whereas the pure kaolinite appears to be formed of slightly larger particles (about 1 µm in the layer plane for the largest) than those observed in natural Sienna.

The specific surface area of pure goethite was measured as 14.7 $m^2$.

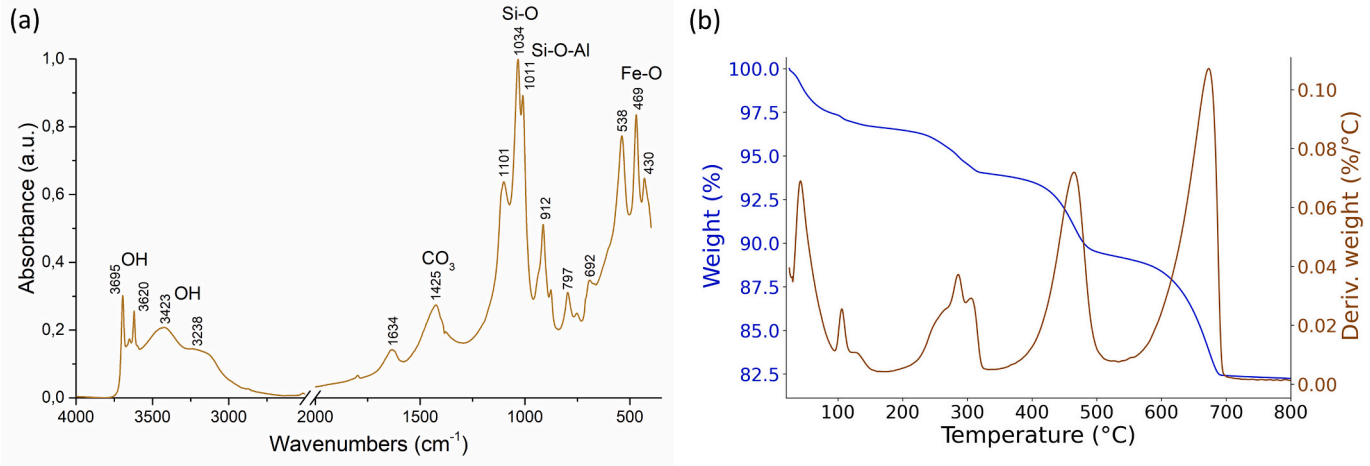


**Fig. 2.** (a) Transmission infrared spectrum of natural Sienna in the region 4000–400 $cm^{-1}$. (b) TG-DTA curves of Sienna.

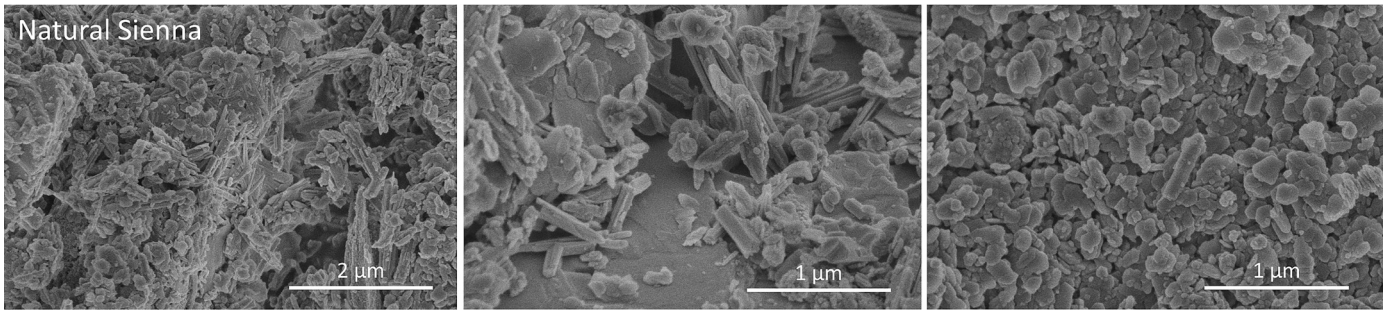


**Fig. 4.** SEM photos of natural Sienna.

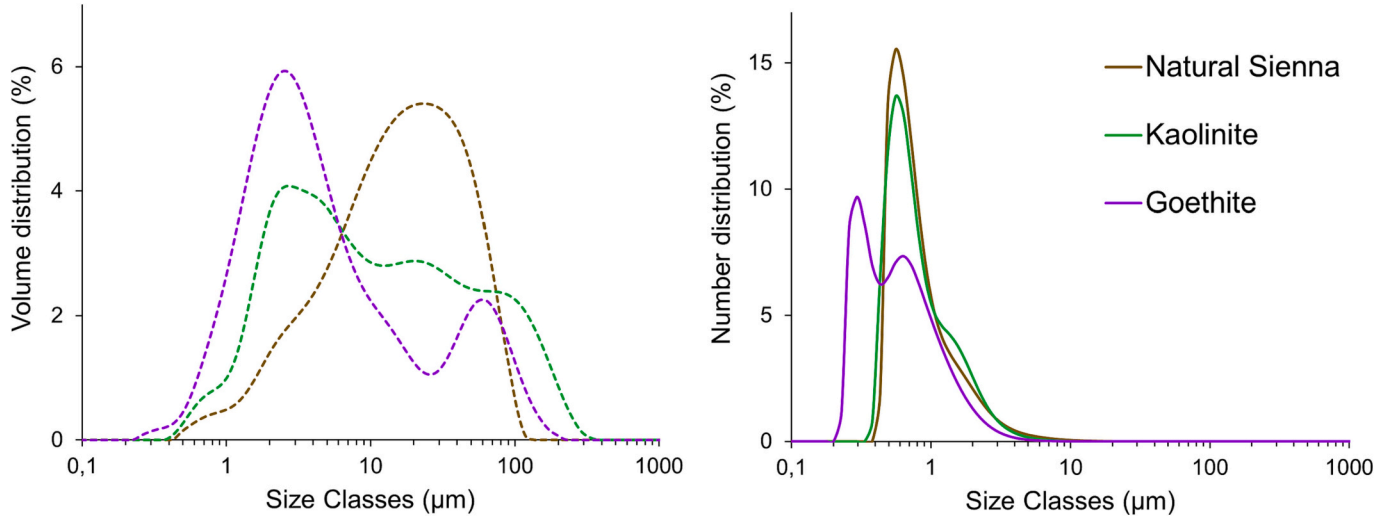


**Fig. 5.** Size distribution in volume (left) and in number (right) of particles in Sienna (brown curve), pure kaolinite (green curve) and pure goethite (purple curve) in water. (For interpretation of the references to colour in this figure legend, the reader is referred to the web version of this article.)

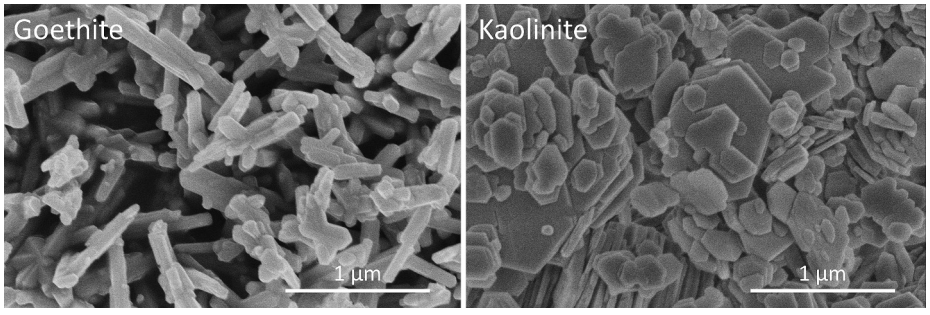


**Fig. 6.** SEM photos of pure goethite and pure kaolinite.

$g^{-1}$ and the SSA of pure kaolinite is reported by the supplier as 10.1 $m^2.g^{-1}$, whereas for STx-1 montmorillonite a SSA of 83.8 $m^2.g^{-1}$ is indicated.

At first sight, in terms of morphological features, pure kaolinite and pure goethite thus appear as proper models for understanding the properties of natural Sienna employed as pigment in tempera paint.

### 3.2. Adsorption of the binder on the pigment

In order to get more insight into the effect of binder in egg yolk-based tempera paints, it seems relevant to examine the adsorption of binder molecules onto pigment particles. Egg yolk is mainly composed of water (around 50%), lipids (around 30%), and proteins (around 15%). The remaining 5% correspond to carbohydrates, minerals, colored molecules and vitamins (Phenix, 1997; Anton, 2007, 2013; Xiao et al., 2020). The main phospholipid present in yolk, phosphatidylcholine, generally referred to as lecithin accounts for 12% of dry matter of yolk (Phenix, 1997). We therefore chose in a first step to use lecithin and studied its adsorption onto natural Sienna and some of its component minerals.

The isotherm adsorption of lecithin on natural Sienna (brown squares in Fig. 7) exhibits a sharp increase at low equilibrium concentration followed by a plateau at $Q_{Sienna} = 0.16$ g/g for lecithin concentration > 10 mmol/L. Such a shape is indicative of a high affinity of lecithin towards Sienna earth. Looking at the individual components, it appears that the isotherm corresponding to kaolinite displays a similar shape with a plateau around $Q_{kaolinite} = 0.03$ g/g (green triangles in Fig. 7), whereas the isotherm for goethite exhibits a low adsorbed amount at low equilibrium concentration followed by a steady increase

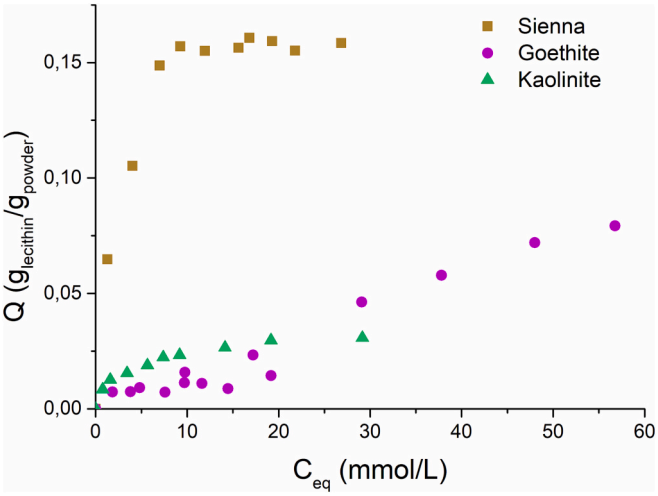


**Fig. 7.** Adsorption isotherms of lecithin on natural Sienna (brown squares), on goethite (purple circles) and on kaolinite (green triangles): evolution of the adsorbed charge of lecithin Q in function of the equilibrium concentration of lecithin $C_{eq}$. (For interpretation of the references to colour in this figure legend, the reader is referred to the web version of this article.)

of the amount adsorbed. This latter result is rather surprising, as goethite is known to have a strong affinity towards phosphate groups (Chitrakar et al., 2006; Luengo et al., 2006; Zhong et al., 2007), even in natural materials (Torrent, 1992). However, when looking at the structure of lecithin, it appears that the phosphate groups in lecithin may not be easily accessible since the phosphate is bound to a choline and a glycerol moieties. Furthermore, lecithin is positively charged on the choline group (Li et al., 2023), which could explain its low affinity for goethite that has an isoelectric point around 7.0. Still, adsorption isotherms here were carried out in ethanol and such reasoning may not fully apply.

All these results tend to show that lecithin adsorption on natural Sienna is likely dominated by adsorption onto clay fractions. Such an interpretation is reinforced by the fact that the specific surface area ratio between pure kaolinite (≈10 $m^2.g^{-1}$) and natural Sienna (≈50 $m^2.g^{-1}$) is very close to the adsorbed amount ratio of lecithin between the two systems. Furthermore, the shape of the adsorption isotherm with a plateau highlights saturation of the adsorbed lecithin charge. Considering a surface headgroup of the lecithin molecule of 0.58 $nm^2$, the saturation value corresponds to the charge of almost two layers of lecithin molecules absorbed on Sienna and kaolinite. This would suggest a bilayer adsorption, which has been reported in the literature for intercalation between bentonite sheets (Li et al., 2023).". Still, it is rather difficult to obtain a full quantitative picture of lecithin adsorption on natural Sienna considering that the surface areas of the various components in the complex system is not known. Moreover, goethite in natural Sienna is not equivalent to the pure goethite used in our study. Indeed, detailed analysis of the diffractogram have shown that most of the goethite present in natural Sienna earth was in fact microcrystalline Al-substituted goethite (Fig. S1).

### 3.3. Solvent accessibility to mineral: NMR relaxometry

As presented above, Sienna earth is composed of several minerals, whose precise chemical composition and proportions vary according to their provenance. We thus decided to prepare a synthetic Sienna by mixing pure minerals (goethite, kaolinite, montmorillonite and calcite) in proportions similar to those determined from the Rietveld refinement of natural Sienna (Table 1) and to compare their behavior as paints, as well as those of the individual minerals. For montmorillonite, we chose to use the STx-1 sample from the Clay Minerals Society as it is a classical representative of a $Ca^{2+}$ exchanged montmorillonite. Amorphous phases were replaced by calcite.

An important feature to understand paint behavior is to assess the proportion of pigment surfaces that are actually accessible to solvent molecules, i.e. in this case mainly water and lipoprotein molecules. NMR relaxometry is a perfectly suited tool for probing such phenomena as it provides information on the multiscale dynamics of molecules (Kimmich, 1997; Korb, 2018). In particular, measuring the NMR relaxation rate $R_1 = 1/T_1$ of $^1H$ at Larmor frequency spanning from 0.01 to 30 MHz, provide insights into the dynamics of water and lipoproteins in the vicinity of mineral surfaces, and into their interactions with surface atoms (Cooper et al., 2013; Yuan et al., 2017; Fanost et al., 2021).

Fig. 8 shows the $^1H$ NMR relaxation dispersion (NMRD) profiles of tempera paints pigmented with the main mineral components of Sienna (goethite, kaolinite, montmorillonite), and of both natural and reconstituted Sienna earths. The relaxation rate $R_1$ at each frequency is determined by the fitting of the magnetization curves by exponential decays. Here, two populations of protons have been identified, a fast relaxation rate named $R_{1\_fast}$ and a slow one named $R_{1\_slow}$. The profiles of the fast population of the five minerals differ from each other. Peaks are visible at 2–4 MHz corresponding to $^1H$—$^{14}N$ quadrupolar peaks (Kimmich, 1977; Fanost et al., 2022) assessing the presence of poorly mobile proteins. Conversely, $R_{1\_slow}$ curves are similar for all mineral components. Quadrupolar peaks are also present assessing the presence of more mobile proteins. $R_{1\_fast}$ represent 70% of the signal relaxation and $R_{1\_slow}$ the remaining 30% which is close to the proportions respectively of water $^1H$ and of lipoproteins $^1H$ contained in the tempera binder. Consequently, $R_{1\_fast}$ can be attributed to the relaxation rates of water $^1H$ in the vicinity of proteins and $R_{1\_slow}$ to the lipoproteins $^1H$.

To go further in the understanding of the interactions between the solvent and the pigment, NMRD profiles of aqueous dispersions of the mineral components have been recorded without egg yolk (Fig. S5). Similarly to Fanost et al. (2022), magnetization curves have mono-exponential dependence. The shape of the NMRD profiles of aqueous dispersions is very similar to the $R_{1\_fast}$ curves (corresponding to interactions with water $^1H$) in tempera dispersions. This is a strong confirmation that $R_{1\_fast}$ corresponds to water in the vicinity of mineral in the tempera paint. Again, the different suspensions display significantly different NMRD profiles that seem to be mineral-specific, as reported by Fanost et al. (2021) in the case of green earth pigments. The curve corresponding to goethite is the one that exhibits the highest $R_1$ values over the whole frequency range. This is linked to the presence in this sample of high amounts of paramagnetic species, mainly Fe(III). The more Fe(III) is present in a mineral, the higher its $R_1$ value (Helm, 2006). Furthermore, in the case of goethite, the magnetic moment of Fe(III) are aligned yielding to a super magnetic moment with a strong magnetic anisotropy (magnetic moment blocked on the structural axis of the particle) (Mørup et al., 1983; Dekkers, 1989; Bocquet et al., 1992). The NMRD profile of goethite (Fig. 8 and Fig. S5) is characteristic of such magnetic particles. Curves corresponding to clay minerals, i.e. kaolinite and montmorillonite display a significantly different shape with a smooth and steady decreases of $R_1$ with frequency. Furthermore, the profile corresponding to montmorillonite is located at higher $R_1$ values than that of kaolinite. Such a difference can be assigned to the difference in surface area between those two phyllosilicates. Indeed, $R_1$ is sensitive to the amount of surface accessible to water (the higher the surface, the higher $R_1$).

In multicomponent systems, the NMRD profiles of a suspension formed with a mixture of minerals is equal to the sum of the NMRD profiles of each component weighted by its proportion in the mixture (Fanost et al., 2021). This is indeed the case for the profile of the reconstituted Sienna up to 3 MHz. Comparing the latter with that of natural Sienna, both profiles are almost superimposed at low frequencies. This is even more evident considering the NMRD profiles in tempera binder (Fig. 8). However, for frequencies higher than 3 MHz, a marked difference in shape can be observed. Indeed, the $R_1$ curve corresponding to natural Sienna exhibit a slighter decrease of $R_1$ at high

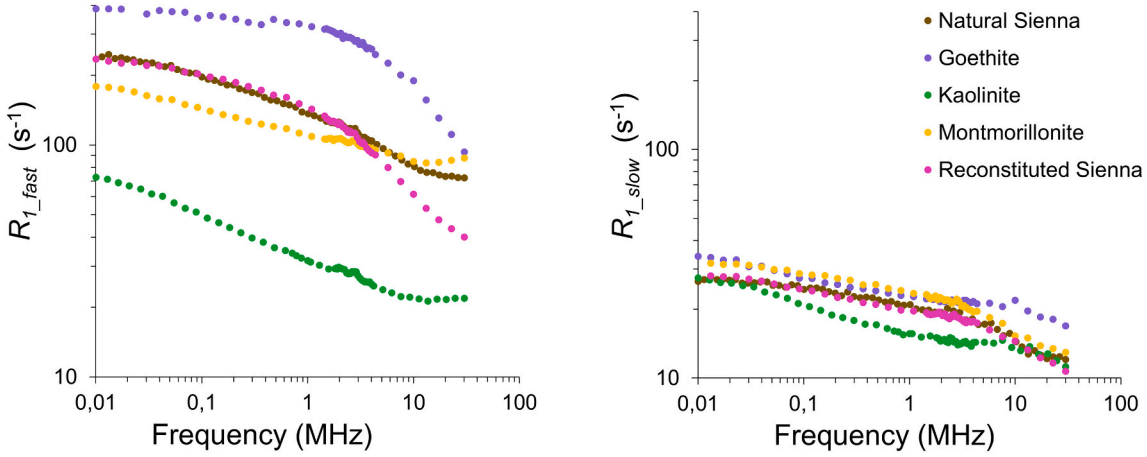


**Fig. 8.** Relaxation rates ($R_1$) for tempera paints. Left: $R_{1\_fast}$ and right: $R_{1\_slow}$, obtained from biexponential fit of the magnetization decays.

frequency than reconstituted Sienna which shows a goethite-like shape. Such a difference could be assigned to a non-accessibility of water to goethite in the natural sample but, in view of the morphological features described above, this appears rather unlikely. Another explanation could be found in the crystal-chemistry of goethite revealed by X-ray diffraction, most of which being Al-substituted. Such crystal chemistry significantly decreases the amount of structural paramagnetic atoms, which could explain the observed difference in profile shapes (Fig. 8 and Fig. S5). In any case, this shows that defining proper model systems able to reproduce natural samples requires a thorough mineralogical, crystal-chemical, and morphological characterization of the natural samples as subtle variations in crystal chemistry or texture may have a significant impact on some properties.

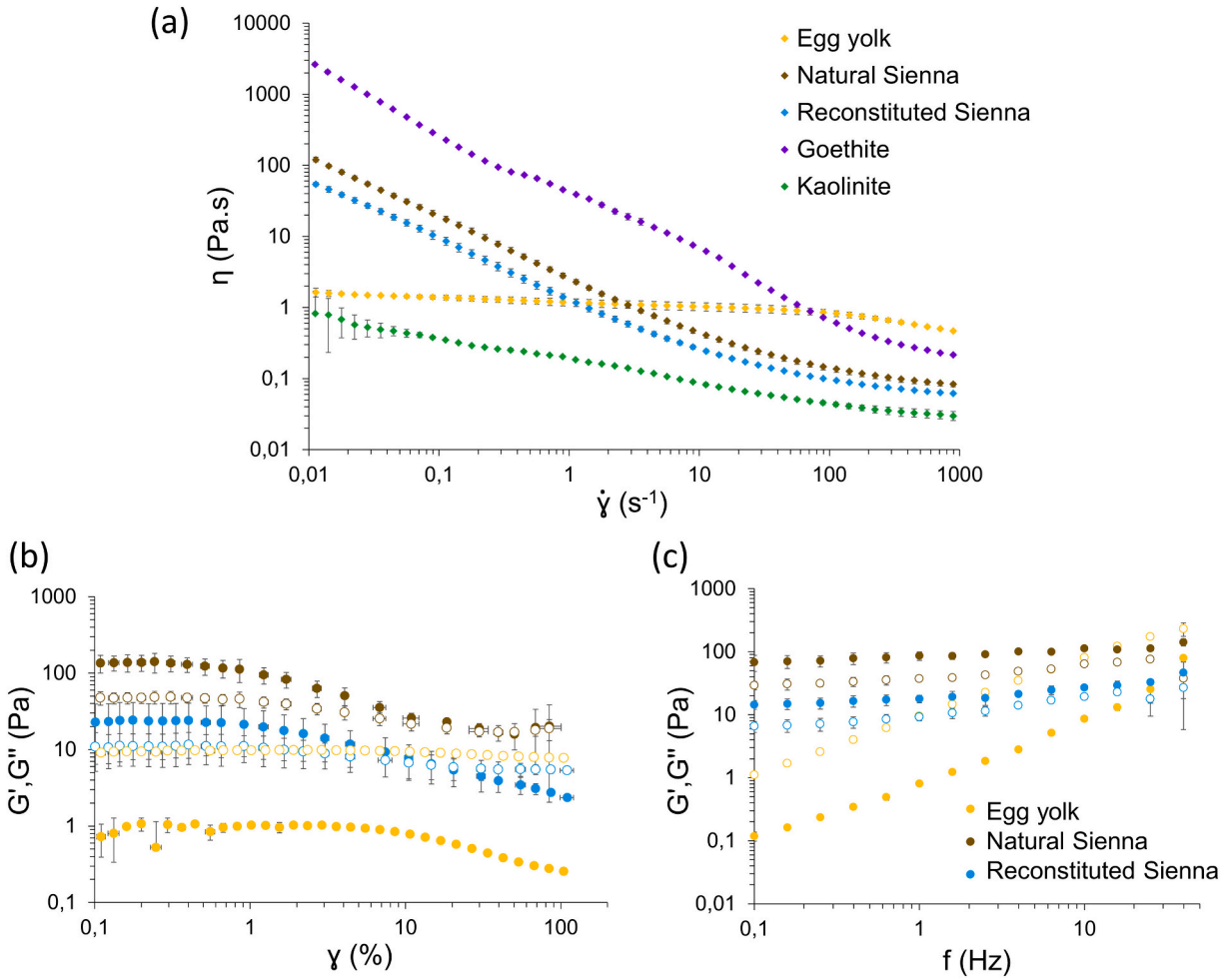


**Fig. 9.** Rheological measurements of egg yolk and tempera paints with natural Sienna and reconstituted Sienna. For comparison with pure minerals, flow measurements of paint preparations with goethite and kaolinite are plotted. Flow measurements (a), strain sweep (b) and frequency sweep (c). G' in full circles and G" in empty circles. Error bars for 2 measurements of the same paint.

### 3.4. Formulation of tempera paints: effect of the mineral on rheological properties of paints

Rheological properties give insights into the consistency and texture of paints from low solicitation to high deformation, corresponding to the flow under the painter's brush. Tempera paints prepared with natural Sienna are stable in time as no significant sedimentation is observed during the time of use, which may be due to swelling clays present in natural Sienna, such as montmorillonite.

Fig. 9a displays the flow curves of tempera prepared with kaolinite and goethite, and those of both natural and reconstituted Siennas. The flow curve of pure egg yolk is also plotted as a reference. Egg yolk exhibits a low viscosity (≈ 1 Pa s) and a moderate shear thinning in agreement with previous studies (Fanost, 2019). Kaolinite and goethite-based tempera formulae both display a much more pronounced shear thinning behavior. For the same mass fraction, and despite a lower volume fraction, goethite suspension exhibits a viscosity much higher than that of the kaolinite suspension. This difference may be due to the differences in size and shape between both samples (Mueller et al., 2010; Puisto et al., 2012), goethite being smaller and more anisotropic (Fig. 5 and Fig. 6). Tempera paints based on both natural and reconstituted Siennas exhibit a flow behavior intermediate between those of their two main components, i.e. kaolinite and goethite. Furthermore, the viscosity of the natural sample is slightly higher than that of its reconstituted counterpart, which can be due to the higher specific surface area of natural Sienna that possibly allows for more interactions between the pigment and the binder. It is worth pointing out the fact that shear thinning is a required property for industrial paints, and can therefore be a feature of interest for artists. Indeed, for low shear rates, a high viscosity is needed to prevent settling and dripping after application, while for shear rates between 100 and 1000 $s^{-1}$, corresponding to the shear rates exerted by a painter's brush, the viscosity should be low enough to allow easy flow and spreading (Larson et al., 2022). Dynamic oscillatory measurements confirm a different behavior between pure binder and paint formulations (Fig. 9b and 10c). The strain sweep measurements of pure egg yolk (Fig. 9b) reveal a liquid-like behavior whatever the applied strain with a viscous modulus (G") higher than the elastic one (G'). Conversely, at low strain (from 0.1 to 1%), tempera paints prepared with both natural and reconstituted Siennas display viscoelastic properties with G' values significantly higher than G". The Linear Visco-Elastic Region (LVER) extends up to strains of 1%. G' and G" intersect at the critical strain (for $\gamma \approx 20\%$), which is a characteristic behavior of suspension pastes and a feature common to numerous paint formulations (Salvant Plisson et al., 2014). In agreement with flow measurements, for the same volume fraction, the elastic and viscous moduli of formulae based on natural Sienna are slightly higher than those of the reconstituted sample.

Frequency sweep measurements (Fig. 9c) were carried out in the LVER for an applied stress of 0.1 Pa, i.e. a strain of $\gamma \approx 0.1\%$. Whereas both G' and G" increase with frequency for pure egg yolk, the curves corresponding to natural and reconstituted Sienna samples exhibit constant G' and G" values independent of the applied frequency, which tends to a gel-like behavior. All these experiments suggest that the main rheological features of tempera based on natural Sienna are well captured by using a model system, despite the imperfection of the present one.

## 4. Conclusion

This paper proposes a detailed investigation of egg-tempera paint based on Sienna earth, a very common pigment of complex composition, focusing first on the pigment composition, then probing its physico-chemical properties in interaction with the binder. Different systems were monitored, considering either historical reconstructions (natural Sienna earth and egg yolk), simplified model systems (with lecithin and a synthetic Sienna earth) or even the pure components of the pigment. Interactions between lecithin and Sienna or its main constituents were studied. The high amount of the surfactant adsorbed on Sienna compared to kaolinite and goethite highlighted probably the synergy between all minerals constituting natural Sienna. Relaxation rates measured on the different minerals in water pointed out that Sienna is a complex microstructure that cannot result from a simple physical mix of pure minerals, even though the rheological properties might suggest the opposite. Due to the complexity of modelling the behavior of tempera paint, the relevance of the models proposed depends on the scale of the properties studied: for macroscopic properties, it seems that reconstituted Sienna fits well with the natural one while at the mesoscopic scale, systems should be chosen carefully. All in all, the composition of the pigment is of great importance while mixing with the binder, allowing the artist to give the desired texture to its paint based on rheological properties.

## CRediT authorship contribution statement

**Floriane Gerony:** Investigation, Data curation, Formal analysis, Writing – original draft. **Laurence de Viguerie:** Conceptualization, Formal analysis. **Côme Thillaye du Boullay:** Formal analysis. **Fabrice Gaslain:** Formal analysis. **Bruno Lanson:** Formal analysis. **Camille Colin:** Investigation. **Laurent Michot:** Methodology, Writing – original draft. **Anne-Laure Rollet:** Methodology, Supervision, Writing – review & editing. **Guillaume Mériguet:** Conceptualization, Supervision, Writing – review & editing. **Maguy Jaber:** Conceptualization, Methodology, Supervision, Writing – review & editing, Funding acquisition.

## Declaration of competing interest

We declare that this manuscript is original, has not been published before and is not currently being considered for publication elsewhere. We declare no conflicts of interest associated with this publication. In addition, we, the authors declare that the manuscript was prepared strictly according to the Journal format.

We have approved the manuscript and agreed with its submission to Applied Clay Science.

This work was supported by the *Observatoire des patrimoines de l'Alliance Sorbonne Université* (OPUS).

## Data availability

Data will be made available on request.

## Appendix A. Supplementary data

Supplementary data to this article can be found online at https://doi.org/10.1016/j.clay.2023.107236.

## References

Anoardo, E., Galli, G., Ferrante, G., 2001. Fast-field-cycling NMR: applications and instrumentation. Appl. Magn. Reson. 20, 365–404. https://doi.org/10.1007/BF03162287.

Anton, M., 2007. Composition and Structure of Hen Egg Yolk. In: Huopalahti, R., López-Fandiño, R., Anton, M., Schade, R. (Eds.), Bioactive Egg Compounds. Berlin, pp. 1–6.

Anton, M., 2013. Egg yolk: structures, functionalities and processes: egg yolk: structures, functionalities and processes. J. Sci. Food Agric. 93, 2871–2880. https://doi.org/10.1002/jsfa.6247.

Bikiaris, D., Daniilia, S., Sotiropoulou, S., Katsimbiri, O., Pavlidou, E., Moutsatsou, A.P., Chryssoulakis, Y., 2000. Ochre-differentiation through micro-Raman and micro-FTIR spectroscopies: application on wall paintings at Meteora and Mount Athos, Greece. Spectrochim. Acta A Mol. Biomol. Spectrosc. 56, 3–18. https://doi.org/10.1016/S1386-1425(99)00134-1.

Bocquet, S., Pollard, R.J., Cashion, J.D., 1992. Dynamic magnetic phenomena in fine-particle goethite. Phys. Rev. B 46, 11657–11664. https://doi.org/10.1103/PhysRevB.46.11657.

Brouillette, C.G., Segrest, J.P., Ng, T.C., Jones, J.L., 1982. Minimal size phosphatidylcholine vesicles: effects of radius of curvature on head group packing

and conformation. Biochemistry 21, 4569–4575. https://doi.org/10.1021/bi00262a009.
Cennini, C., Broecke, L., 2015. Cennino Cennini's Il Libro dell'arte: A New English Translation and Commentary with Italian Transcription. Archetype Publications, London.
Chitrakar, R., Tezuka, S., Sonoda, A., Sakane, K., Ooi, K., Hirotsu, T., 2006. Phosphate adsorption on synthetic goethite and akaganeite. J. Colloid Interface Sci. 298, 602–608. https://doi.org/10.1016/j.jcis.2005.12.054.
Clarke, M., 2011. Mediaeval painters' Materials and Techniques: The Montpellier Liber Diversarum Arcium. Archetype, London.
Cooper, C.L., Cosgrove, T., van Duijneveldt, J.S., Murray, M., Prescott, S.W., 2013. The use of solvent relaxation NMR to study colloidal suspensions. Soft Matter 9, 7211. https://doi.org/10.1039/c3sm51067k.
De L'escalopier, C., 1977. Théophile Prètre et Moine, Essai Sur Divers Arts, Libr. des Arts et métiers-Ed. J. Laget. ed.
Dekkers, M.J., 1989. Magnetic properties of natural goethite-I. Grain-Size dependence of some low- and high-field related rockmagnetic parameters measured at room temperature. Geophys. J. Int. 97, 323–340. https://doi.org/10.1111/j.1365-246X.1989.tb00504.x.
Doebelin, N., Kleeberg, R., 2015. Profex: a graphical user interface for the Rietveld refinement program BGMN. J. Appl. Crystallogr. 48, 1573–1580. https://doi.org/10.1107/S1600576715014685.
Fanost, A., 2019. Formulation et propriétés physico-chimiques de peintures a tempera à base de jaune d'œuf et de terres vertes. Ph.D. dissertation. Sorbonne Université, Paris.
Fanost, A., Jaber, M., de Viguerie, L., Korb, J.-P., Levitz, P.E., Michot, L.J., Mériguet, G., Rollet, A.-L., 2020. Green Earth pigments aqueous dispersions: NMR relaxation rates dataset. Data Brief 32, 106270. https://doi.org/10.1016/j.dib.2020.106270.
Fanost, A., Jaber, M., de Viguerie, L., Korb, J.-P., Levitz, P.E., Michot, L.J., Mériguet, G., Rollet, A.-L., 2021. Green earth pigments dispersions: Water dynamics at the interfaces. J. Colloid Interface Sci. 581, 644–655. https://doi.org/10.1016/j.jcis.2020.07.085.
Fanost, A., de Viguerie, L., Ducouret, G., Mériguet, G., Walter, P., Glanville, H., Rollet, A.-L., Jaber, M., 2022. Connecting rheological properties and molecular dynamics of egg-tempera paints based on egg yolk. Angew. Chem. Int. Ed. 61, e202112108 https://doi.org/10.1002/anie.202112108.
Genestar Juliá, C., Pons Bonafé, C., 2004. The use of natural earths in picture: study and differentiation by thermal analysis. Thermochim. Acta 413, 185–192. https://doi.org/10.1016/j.tca.2003.10.016.
Genestar, C., Pons, C., 2005. Earth pigments in painting: characterisation and differentiation by means of FTIR spectroscopy and SEM-EDS microanalysis. Anal. Bioanal. Chem. 382, 269–274. https://doi.org/10.1007/s00216-005-3085-8.
Grygar, T., Hradilová, J., Hradil, D., Bezdička, P., Bakardjieva, S., 2003. Analysis of earthy pigments in grounds of Baroque paintings. Anal. Bioanal. Chem. 375, 1154–1160. https://doi.org/10.1007/s00216-002-1708-x.
Helm, L., 2006. Relaxivity in paramagnetic systems: theory and mechanisms. Prog. Nucl. Magn. Reson. Spectrosc. 49, 45–64. https://doi.org/10.1016/j.pnmrs.2006.03.003.
Helwig, K., 1998. The characterisation of iron earth pigments using infrared spectroscopy. In: IRUG$^2$ VA Postprints, pp. 83–92.
Hradil, D., Grygar, T., Hradilová, J., Bezdička, P., 2003. Clay and iron oxide pigments in the history of painting. Appl. Clay Sci. 22, 223–236. https://doi.org/10.1016/S0169-1317(03)00076-0.
Israelachvili, J.N., 2011. Intermolecular and Surface Forces, 3rd ed. Academic press, Burlington (Mass.).
Kimmich, R., 1977. Nuclear magnetic relaxation in the presence of quadrupole nuclei. Z. Für Naturforschung A 32, 544–554. https://doi.org/10.1515/zna-1977-0604.
Kimmich, R., 1997. NMR. Springer Berlin Heidelberg, Berlin, Heidelberg. https://doi.org/10.1007/978-3-642-60582-6.
Korb, J.-P., 2018. Multiscale nuclear magnetic relaxation dispersion of complex liquids in bulk and confinement. Prog. Nucl. Magn. Reson. Spectrosc. 104, 12–55. https://doi.org/10.1016/j.pnmrs.2017.11.001.
Larson, R.G., Van Dyk, A.K., Chatterjee, T., Ginzburg, V.V., 2022. Associative thickeners for waterborne paints: structure, characterization, rheology, and modeling. Prog. Polym. Sci. 129, 101546. https://doi.org/10.1016/j.progpolymsci.2022.101546.
Laurie, A.P., 1926. The painter's methods & material: The handling of pigments in oil, tempera, water-colour & in mural painting, the preparation of grounds & canvas, & the prevention of discolouration, together with the theories of light & colour applied to the making of pictures. Seeley, Service & Co. Ltd, London.
Li, Q., Berraud-Pache, R., Yang, Y., Souprayen, C., Jaber, M., 2023. Biocomposites based on bentonite and lecithin: an experimental approach supported by molecular dynamics. Appl. Clay Sci. 231, 106751. https://doi.org/10.1016/j.clay.2022.106751.
Luengo, C., Brigante, M., Antelo, J., Avena, M., 2006. Kinetics of phosphate adsorption on goethite: comparing batch adsorption and ATR-IR measurements. J. Colloid Interface Sci. 300, 511–518. https://doi.org/10.1016/j.jcis.2006.04.015.
Manasse, A., Mellini, M., 2006. Iron (hydr)oxide nanocrystals in raw and burnt sienna pigments. Eur. J. Mineral. 18, 845–853. https://doi.org/10.1127/0935-1221/2006/0018-0845.
Manea, M.M., Moise, I.V., Virgolici, M., Negut, C.D., Barbu, O.-H., Cutrubinis, M., Fugaru, V., Stanculescu, I.R., Ponta, C.C., 2012. Spectroscopic evaluation of painted layer structural changes induced by gamma radiation in experimental models. Radiat. Phys. Chem. 81, 160–167. https://doi.org/10.1016/j.radphyschem.2011.09.015.
Mayer, R., Sheehan, S., 1991. The Artist's Handbook of Materials and Techniques, 5th ed., rev.Updated. ed. Viking, New York, N.Y., U.S.A.
Mazzeo, R., Prati, S., Quaranta, M., Joseph, E., Kendix, E., Galeotti, M., 2008. Attenuated total reflection micro FTIR characterisation of pigment–binder interaction in reconstructed paint films. Anal. Bioanal. Chem. 392, 65–76. https://doi.org/10.1007/s00216-008-2126-5.
Meilunas, R.J., Bentsen, J.G., Steinb, A., 1990. Analysis of Aged Paint Binders by FTIR Spectroscopy, p. 20.
Merrifield, M.P. (Ed.), 1999. Medieval and Renaissance Treatises on the Arts of Painting: Original Texts with English Translations. Dover Publications, Mineola, N.Y.
Mørup, S., Bo Madsen, M., Franck, J., Villadsen, J., Koch, C.J.W., 1983. A new interpretation of Mössbauer spectra of microcrystalline goethite: "super-ferromagnetism" or "super-spin-glass" behaviour? J. Magn. Magn. Mater. 40, 163–174. https://doi.org/10.1016/0304-8853(83)90024-0.
Mueller, S., Llewellin, E.W., Mader, H.M., 2010. The rheology of suspensions of solid particles. Proc. R. Soc. Math. Phys. Eng. Sci. 466, 1201–1228. https://doi.org/10.1098/rspa.2009.0445.
Navas, N., Romero-Pastor, J., Manzano, E., Cardell, C., 2010. Raman spectroscopic discrimination of pigments and tempera paint model samples by principal component analysis on first-derivative spectra. J. Raman Spectrosc. 41, 1486–1493. https://doi.org/10.1002/jrs.2646.
Phenix, A., 1997. The composition and chemistry of eggs and egg tempera. In: Early Italian Paintings: Techniques and Analysis. Maastricht, pp. 11–20.
Puisto, A., Illa, X., Mohtaschemi, M., Alava, M.J., 2012. Modeling the viscosity and aggregation of suspensions of highly anisotropic nanoparticles. Eur. Phys. J. E: Soft Matter Biol. Phys. 35, 6. https://doi.org/10.1140/epje/i2012-12006-1.
Romero-Pastor, J., Cardell, C., Manzano, E., Yebra-Rodríguez, Á., Navas, N., 2011. Assessment of Raman microscopy coupled with principal component analysis to examine egg yolk-pigment interaction based on the protein C-H stretching region (3100–2800 cm $^{-1}$): Multivariate Raman study of egg yolk-pigment interaction. J. Raman Spectrosc. 42, 2137–2142. https://doi.org/10.1002/jrs.2977.
Salvant Plisson, J., de Viguerie, L., Tahroucht, L., Menu, M., Ducouret, G., 2014. Rheology of white paints: how Van Gogh achieved his famous impasto. Colloids Surf. A Physicochem. Eng. Asp. 458, 134–141. https://doi.org/10.1016/j.colsurfa.2014.02.055.
Schulze, D.G., 1984. The influence of aluminum on iron oxides. VIII. Unit-cell dimensions of al-substituted goethites and estimation of Al from them. Clay Clay Miner. 32, 36–44. https://doi.org/10.1346/CCMN.1984.0320105.
Schwertmann, U., Carlson, L., 1994. Aluminum influence on iron oxides: XVII. Unit-cell parameters and aluminum substitution of natural goethites. Soil Sci. Soc. Am. J. 58, 256–261. https://doi.org/10.2136/sssaj1994.03615995005800010039x.
Schwertmann, U., Cornell, R.M. (Eds.), 2000. Iron Oxides in the Laboratory: Preparation and Characterization. Wiley-VCH Verlag GmbH, Weinheim, Germany. https://doi.org/10.1002/9783527613229.
Thompson, D.V., York, L.E., 1962. The practice of tempera painting: materials and methods, unabridged republication of the work originally published in 1936. ed. Dover books on art instruction, anatomy, Dover, New York.
Torrent, J., 1992. Fast and slow phosphate sorption by goethite-rich natural materials. Clay Clay Miner. 40, 14–21. https://doi.org/10.1346/CCMN.1992.0400103.
Xiao, N., Zhao, Y., Yao, Y., Wu, N., Xu, M., Du, H., Tu, Y., 2020. Biological activities of egg yolk lipids: a review. J. Agric. Food Chem. 68, 1948–1957. https://doi.org/10.1021/acs.jafc.9b06616.
Yuan, L., Chen, L., Chen, X., Liu, R., Ge, G., 2017. *In situ* measurement of surface functional groups on silica nanoparticles using solvent relaxation nuclear magnetic resonance. Langmuir 33, 8724–8729. https://doi.org/10.1021/acs.langmuir.7b00923.
Zhong, B., Stanforth, R., Wu, S., Chen, J.P., 2007. Proton interaction in phosphate adsorption onto goethite. J. Colloid Interface Sci. 308, 40–48. https://doi.org/10.1016/j.jcis.2006.12.055.